Impact of air-sea interaction on East Asian summer monsoon climate in WRF

Eun-Jung Kim[1] and Song-You Hong[2]

Received 22 September 2009; revised 24 May 2010; accepted 14 June 2010; published 9 October 2010.

[1] This study investigates the effects of air-sea interaction on the simulated East Asian summer monsoon (EASM) climate in a regional climate model. An ocean mixed layer model with a revised surface roughness length formulation that was originally designed for tropical cyclone simulation and a prognostic sea surface skin temperature scheme that considers the heat budget at the water surface are systematically evaluated on the monsoonal climate over East Asia for July 2006 in the regional Weather Research and Forecasting (WRF) model. Also, 9-year (2000–2008) June–August simulations are performed to evaluate the overall impacts of these three components on the simulated EASM climatology. The 1 month simulation for July 2006 reveals that the inclusion of the ocean mixed layer model cools the water surface due to enhanced mixing, in particular, when winds are strong. Such cooling is largely compensated by the inclusion of prognostic skin temperature since solar heating in daytime overwhelms the cooling in nighttime. The revised surface roughness length effectively reduces the surface heat flux by reducing the exchange coefficients, against the conventional Charnock formula. Consideration of the three components together results in the reduction of systemic biases of excessive precipitation and weakening of the North Pacific high in the summer climate from 2000 to 2008. It is concluded that the methodology designed in this study can be an efficient way to represent the air-sea interaction in regional atmospheric models for numerical weather prediction and climate simulation.

Citation: Kim, E.-J., and S.-Y. Hong (2010), Impact of air-sea interaction on East Asian summer monsoon climate in WRF, *J. Geophys. Res.*, *115*, D19118, doi:10.1029/2009JD013253.

1. Introduction

[2] It is well-known that the sea surface temperature (SST) is a critical component which influences the exchange of energy between the atmosphere and ocean. Since SST influences the atmosphere as well as being controlled by atmospheric conditions, accurate SST information, either from observation or as predicted by a model, can play a crucial part in weather forecasts and climate prediction. However, the spatial and temporal resolution of observed SST data is too poor to describe conditions over the ocean surface accurately. Thus, representation of phenomena that occur in the air-sea interface limits the accuracy of air-sea interaction in atmospheric models. For example, *Fairall et al*. [1996a] have shown that to estimate the heat balance to an accuracy of 10 W m^{-2} requires specification of the SST to an accuracy of ±0.2 K.

[3] Therefore, to approach the real situation it is necessary to represent SST using analysis data adjusted by observed atmospheric data. Researchers have studied various methods to represent SST more realistically. They have found that variation of SST due to wind-driven mixing is one of the significant factors driving air-sea interaction. *De Szoeke* [1980] found that strong wind causes upwelling regions in the ocean because of a deeper mixed layer over which the surface-driven stirring operates, leading to colder surface temperatures in upwelling regions. The ocean mixed layer model is one of the tools which reflect atmospheric effects to the ocean in the form of wind stress, and oceanic effects to the atmosphere by changed SST [*Pollard et al.*, 1972]. The cooled SST reduces surface fluxes and affects atmospheric phenomena such as surface pressure and precipitation. Various ocean mixed layer models have been developed to represent air-sea interaction [*Cherniawsky and Oberhuber*, 1995; *Sutton and Mathieu*, 2002; *Noh et al*, 2002; *Stephens et al.*, 2005].

[4] The diurnal cycle of SST due to the surface energy budget also plays an important role in representing air-sea interactions realistically. *Wilson and Mitchell* [1986] showed that climate models that exclude a diurnal cycle cannot simulate nonlinear processes such as evaporation and partitioning of surface energy into latent and sensible heat fluxes, resulting in degraded model simulations. *Dai and Trenberth* [2004] indicated that when using a fully coupled climate

[1]Numerical Data Assimilation Division, Numerical Prediction Office, Korea Meteorological Administration, Seoul, Korea.
[2]Department of Atmospheric Sciences and Global Environment Laboratory, Yonsei University, Seoul, Korea.

0148-0227/10/2009JD013253

system model, which does not include the diurnal SST variation, simulated diurnal cycles in surface air temperature, pressure, and precipitation over the ocean are much weaker than the observed values. *Shinoda* [2005] found that solar radiation absorbed in the upper few meters significantly influences intraseasonal SST variations through amplitude changes in diurnal SST variation over the western Pacific warm pool. *Fairall et al*. [1996b] and *Zeng and Beljaars* [2005] described some of the physics associated with the diurnal variation of SST, which is composed of the cooling effect of longwave radiation in the cool-skin and a warming effect from solar insolation.

[5] The roughness length over the water body is also a critical factor in determining the heat and momentum exchanges between the atmosphere and water. This formulation does not alter the SST value itself, but directly controls the surface fluxes over the oceans. As the wind speed is higher, the wind stress is also increased [*Charnock*, 1955], which has been widely used in atmospheric models to estimate the roughness length over waters. The Charnock concept has been modified based on observations and theoretical considerations. *Johnson et al*. [1998] studied how wind waves influence momentum transfer between the atmosphere and sea surface, suggesting that wave-age-dependent sea roughness models would be necessary for large-scale models. Further, recent studies have shown that exchange coefficients over water do not increase monotonically, particularly in high wind situations. *Emanuel et al*. [2003] argued that in most cases, uncertainties in environmental wind shear make it difficult to forecast storm intensity accurately. *Donelan et al*. [2004] concluded that measurements of the drag coefficient approach a limiting value in high winds, whereas it has been generally accepted that the drag coefficient increases when the wind speed is less than 20 m s^{-1}. *Powers and Stoelinga* [2000] and *Moon et al*. [2007] further confirmed that parameterized roughness should not be increased in strong wind situations.

[6] The purpose of this study is to investigate the effects of air-sea interaction on the simulated East-Asian summer monsoon (EASM) using a regional climate model (RCM). The EASM is a kind of seasonal circulation that carries warm and moist air from the Indian and Pacific oceans to East Asia and it covers both subtropics and midlatitudes. In the boreal summer, the monsoon advances northward, and induces heavy precipitation (called *Meiyu*, *Baiu*, and *Changma* in China, Japan, and Korea, respectively) over a boundary where the oceanic high pressure system and the continental low pressure system meet across central China, Japan, and Korea. It is certain that the air-sea interaction is very active within the monsoon system over East Asia since many of the precipitation events within the EASM are observed over the oceans. Despite the importance of considering air-sea interactions, there are only a few examples dealing with this phenomenon within the EASM. *Wang et al*. [2005] indicated that the coupled ocean-atmosphere processes in a global climate model (GCM) framework are crucial in the East Asian monsoon regions where atmospheric feedback to SST is critical. *Lee et al*. [2002, 2004] demonstrated that the role of the ocean roughness length is as important as SST in simulations of EASM. Meanwhile, typhoon effects are also important to air-sea interaction because typhoons cause strong wind conditions. However, since we are interested in the effects of air-sea interaction on the East-Asian monsoon and the impact of typhoons on air-sea interaction are secondary interests, we focus on the impact of air-sea interaction on simulated East Asian monsoons in this study.

[7] A model used in this study is the Weather Research and Forecasting (WRF) [*Skamarock et al.*, 2008, hereafter WRF] model. The methods which represent the air-sea interaction in this study include: (1) An ocean mixed layer (OML) model based on *Pollard et al*. [1972] that deals with wind-driven vertical mixing; (2) a prognostic sea surface skin temperature (TDI) scheme based on *Zeng and Beljaars* [2005] that considers SST diurnal variation from the energy budget over the sea surface; and (3) a revised roughness length formulation (DRG) based on *Donelan et al*. [2004] that effectively reduces exchange coefficients in the presence of strong winds. The simulations are performed with National Centers for Environmental Prediction (NCEP) final analysis data (FNL) on 1° × 1° global grids every 6 hours (available at http://dss.ucar.edu/datasets/ds083.2/data/). The month of July 2006, when above-normal precipitation was observed in Korea, is selected to investigate the individual role of the air-sea interaction package in simulating the EASM.

[8] Section 2 describes the experimental setup. In section 3, the results for WRF sensitivities to surface physics parameterization and their evaluations are discussed. Concluding remarks follow in the final section.

2. Model and Experimental Setup

2.1. Model Description

[9] The WRF model is a numerical weather prediction and atmospheric simulation system designed for both research and operational applications. This model is well-suited for cases with real-data initial states and boundary conditions. WRF version 3.0, released in April 2008, is used in this study.

[10] The physics packages used in this study include the WRF single-moment 3-class (WSM3) [*Hong et al.*, 2004] scheme, the Kain-Fritsch cumulus parameterization scheme [*Kain*, 2004], the Noah land-surface model [*Chen and Dudhia*, 2001], the Yonsei University (YSU) planetary boundary layer (PBL) scheme [*Hong et al.*, 2006], a simple cloud-interactive radiation scheme [*Dudhia*, 1989], and the Rapid Radiative Transfer Model (RRTM) for longwave radiation [*Mlawer et al.*, 1997] scheme.

2.2. Methodology

[11] Three components of the surface layer algorithm over water, which correspond to the options available in the WRF model as of May 2009, were evaluated. The first component is an OML model based on *Pollard et al*. [1972]. In the scheme, the mixed layer is deepened and water-cooled due to the wind-driven mixing. As a result, the cooled SST affects the heat and moisture fluxes at the surface when winds are strong. This model omits entrainment and horizontal advection. Further, the model assumes no heat transfer between the individual columns, so that temperature changes within a column can occur only through vertical redistribution. It also does not consider SST warming caused by wind-driven mixing. The mixed layer depth is initialized at 30 m and is updated every 24 hr, which is consistent with the temporal resolution of observed SST.

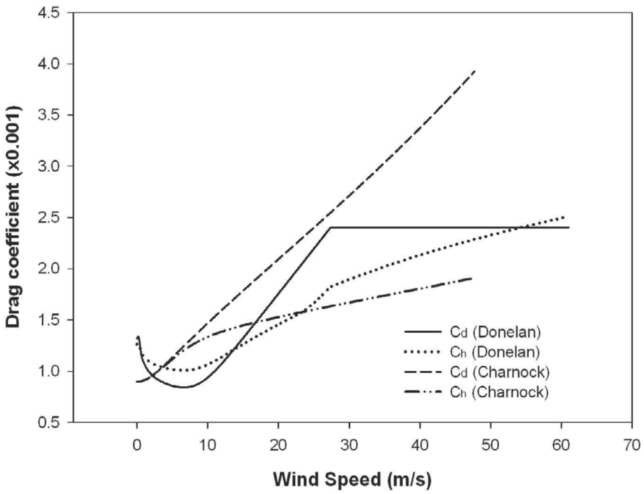

Figure 1. Exchange coefficients as a function of wind speed.

[12] The second component considered is a TDI scheme based on *Zeng and Beljaars* [2005], reflecting the surface energy heat budget over oceanic waters. In ocean-atmosphere coupled models, the term SST refers to the mean temperature of the top ocean layer of about 10 m in depth. SST is significantly different from the sea surface skin temperature since radiative, latent, and sensible heats between the atmospheric and oceanic boundary layers exchange actively [*Fairall et al.*, 1996a]. In this scheme, the skin temperature of the sea surface is calculated by considering the cool skin and warm layer effects due to the net longwave radiation: Latent heat flux, molecular and turbulent mixing processes, and sensible heat flux.

[13] The third component is a DRG formulation based on *Donelan et al.* [2004]. Since the wind stress on the sea surface is a driving force for ocean circulation, accurate representation of the wind stress is important in modeling and forecasting for both atmospheric and oceanic dynamics. Wind stress is parameterized by a drag coefficient C_d or by a roughness length $z_{0\mathrm{m}}$. The drag coefficient can be defined as $C_d = K^2 / (\ln(z_a / z_{0m}))^2$, where K is the Karman constant (0.4) and z_a the surface layer height that is the lowest level of the model. The revised DRG formulae will be evaluated over the *Charnock* [1955] relation, in which the relationship between the mechanical roughness length $z0_\mathrm{m}$ and the frictional velocity u_* is given as $z_{0m} = c_{z_{0m}}\ (\mathrm{u}_*^2 / \mathrm{g}) + \mathrm{o}_{z_{0m}}$, where $c_{z_{0m}} = 0.0185$ and $o_{z_{0m}} = 1.59 \times 10^{-5}$ m. The function for thermal roughness length in computing sensible and latent heat fluxes, z_{0h}, is the same to z_{0m}, but the corresponding similarity function follows the formula of *Carlson and Boland* [1978]. As such, the resulting C_h decreases over C_d as the wind speed increases (Figure 1).

[14] In *Donelan et al.* [2004], z_{0m} is first calculated by $z_{0m} = 10\ \exp(-9 / \mathrm{u}_*^{1/3})$ with an upper limit on z_{0m} of 2.85×10^{-3} m. Then it is recalculated by $z_{0m} = z_{0m} + 0.11 \times 1.5 \times 10^{-5}/\mathrm{u}_*$, with a lower limit on u_* of 0.01 m s^{-1}.

[15] The drag coefficient for winds, $C_{d,}$ is small in the revised formula over the Charnock relation except for calm winds (Figure 1). It is evident that C_d is a constant for winds stronger than 28 m s^{-1} in the new formula, whereas it increases monotonically in the case of the Charnock formula. It is clear that the wind-induced mixing for heat is generally small when the *Donelan et al.* [2004] equation is considered. The exchange coefficient, $C_{h,}$ for the new formula is larger for winds stronger than 24 m s^{-1}, as compared to the value from the default option. The above three components of the surface layer physics over water will be systematically evaluated in this study.

2.3. Experimental Design and Data

[16] Five subsequent experiments were designed. The control experiment (CTL) employs daily SST, as in a typical setup for regional climate simulations, forced by the observed SST and with reanalysis for large-scale forcing [e.g., *Lee et al*, 2007; *Yhang and Hong*, 2008]. The data sets are based on the Optimally Interpolated Sea Surface Temperature (OISST) on a 1° × 1° grid, which utilizes in situ and satellite-derived SSTs plus SSTs simulated by sea ice cover . The weekly OISST was linearly interpolated in time to derive daily values during the integration period.

[17] Each of the following experiments considers the effect of air-sea interaction, which is described above, by replacing an option from the default options used in the CTL experiment. The OML experiment employs an ocean mixed layer model [*Pollard et al.*, 1972]. The TDI and DRG experiments employ a prognostic sea surface skin temperature scheme [*Zeng and Beljaars*, 2005] and a revised roughness length formulation [*Donelan et al.*, 2004], respectively. In the OML and TDI experiments, the SSTs for heat flux computation are modified from the given daily mean SSTs. The SST and initial mixed layer depth are updated daily at 0000 UTC. The initial mixed layer depth is set to 30 m, which is less than 50 m, as in the default value. The reason is as follows. If the mixed layer depth is set deeper, more energy is needed to cool the ocean's mixed layer. In turn, the cooling rate of SST becomes smaller. Consequently, it reduces the wind-driven mixing to reflect its effects. *Bao et al.* [2000] found that the cooling rate is significantly dependent on the initial depth of the ocean mixed layer. *Davis et al.* [2008] used 30 m as the initial mixed layer depth to reflect effectively the wind-driven mixing due to a typhoon. Therefore, we used 30 m as the initial mixed layer depth, as in *Davis et al.* [2008], to account for the mixing effect within a day. The lapse rate used in the OML and the ALL experiments is 0.14 K m^{-1}. The ALL experiment includes all three components (i.e., mixed layer, sea surface skin temperature, and revised roughness length effects).

[18] The WRF model domain covers the East Asian region centered over the Korean peninsula (Figure 2), which is defined in the Lambert conformal space with a 48 km grid (110 × 110 points). The entire grid system has 27 vertical layers with a terrain following the sigma coordinate, and the model top is located at 50 hPa. The single month run for July 2006 is designed to investigate the individual role of three revised physics in forming the EASM circulations. The new physics package combining all three revised physics is evaluated for nine summer periods from 2000 to 2008. For monthly simulations, in order to remove the natural variability of the model, all experiments for July 2006, including the CTL experiment, consist of three ensemble members. Each member is initialized at 0000 UTC on each of 29 June,

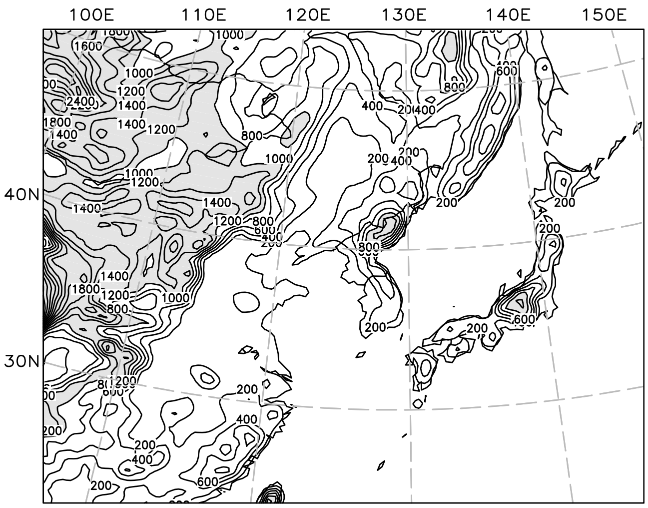

Figure 2. Model domain with terrain heights contoured every 100 m. Terrain heights greater than 1000 m are shaded.

30 June, and 1 July 2006. Preliminary experiments revealed that the magnitude of sensitivities between each ensemble member does not differ in terms of monthly and seasonal climatology, which is also consistent with the results from *Kang and Hong* [2008]. In this study we used the analyzed results during 0000 UTC on July to 0000 UTC on 01 August. The observed precipitation dataset for verification of the model results is the Tropical Rainfall Measuring Mission (TRMM) Multi-satellite Precipitation Analysis (TMPA) on 0.25° × 0.25° global grids every 3hours [*Huffman et al.*, 2007].

[19] Figure 3 represents the monthly averaged characteristics of synoptic features for the selected summer and winter monsoons. In July 2006, a maritime high pressure system over the northwestern Pacific, a continental high centered in Mongolia, and a low pressure belt extending northeastward from south China constitute a typical distribution of atmospheric pressure in East Asia in summer (Figure 3a). Southerly or southwesterly flows along the western periphery of the maritime transport warm and moist air to Korea and Japan. The monsoonal rain band extending northeastward from southern China to the Korean peninsula and Japan is typical in July (Figure 3b).

3. Results

[20] In section 3.1, results from the CTL experiment are described. Section 3.2 describes the influence of individual components (e.g., the OML model, the TDI scheme, and the DRG formulation) on the simulated EASM. The impact of the air-sea interaction package on the simulated climatology (2000–2008) is discussed in section 3.3.

3.1. Control Simulations (July 2006)

[21] The CTL experiment well-simulates the North Pacific high pressure system, with the 850 hPa southwesterly winds transporting warm and moist air from south China to Korea (Figure 4a). It is, however, shown that the model tends to underestimate pressure in China and the northwestern Pacific Ocean. An increase in pressure is

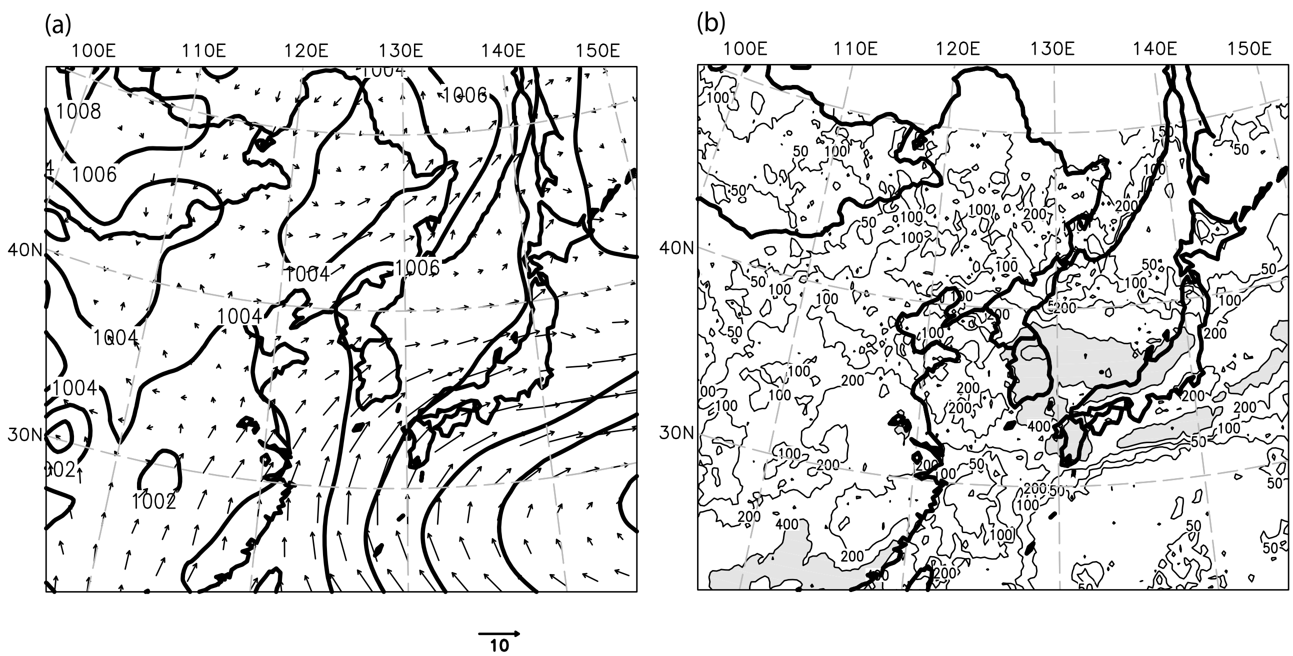

Figure 3. (a) Monthly sea level pressure (hPa) and 850 hPa wind (vector) for July 2006 obtained from the National Centers for Environmental Prediction (NCEP) Final Analysis (FNL) data. (b) The corresponding precipitation (mm) from the Tropical Rainfall Measuring Mission (TRMM) Multi-satellite Precipitation Analysis (TMPA) data. Shaded areas in (b) are for precipitation over 400 mm.

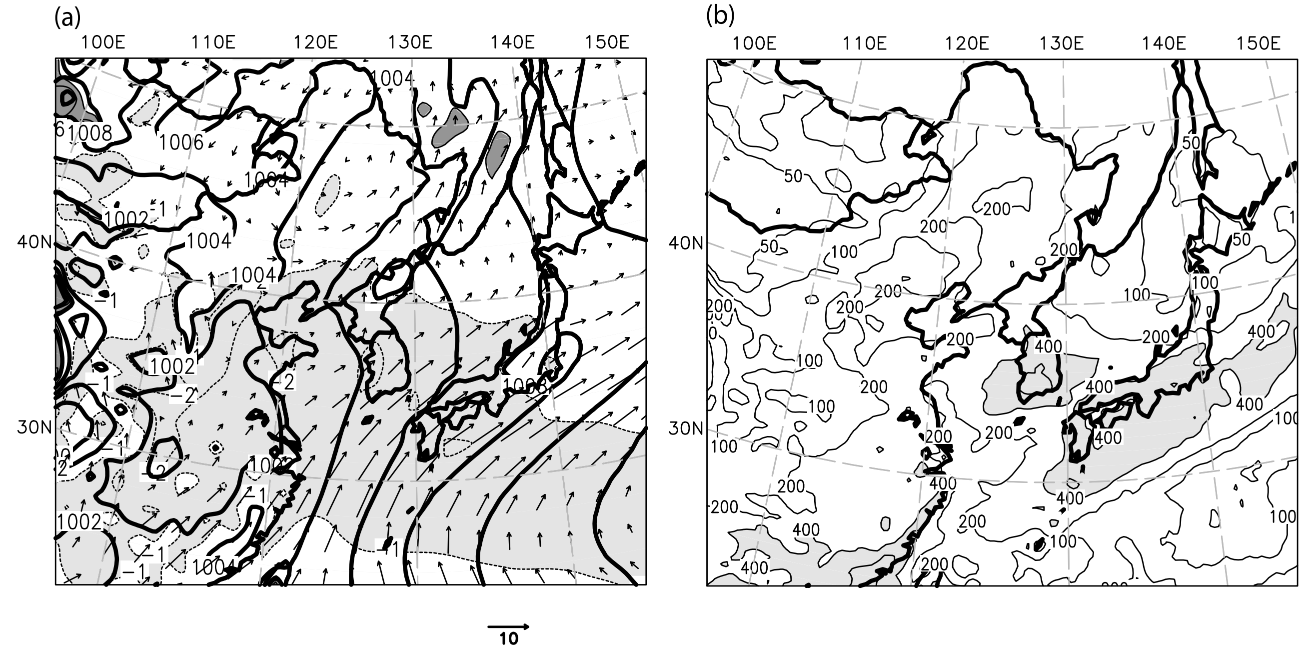

Figure 4. (a) Monthly sea level pressure (mb, solid line) for July 2006 obtained from the control (CTL) experiment and the corresponding difference (CTL minus FNL, shaded) with 850 hPa wind (vector) obtained from the CTL experiment. (b) The corresponding precipitation (mm) obtained from the CTL experiment in July 2006. Shaded areas in Figure 4a indicate the differences in averaged sea level pressure over 1 hPa and in Figure 4b indicate differences in accumulated precipitation of over 400 mm.

evident in the western part of Siberia. The relatively larger errors in areas near the western boundary of the domain are distinct, which seem to be due to the incorrect treatment of model dynamics over areas of steep orography. The WRF model is capable of simulating the monsoonal precipitation (Figure 4b). For example, the monsoonal precipitation stretching from South China to the northeast is fairly-well-reproduced (see Figures 3b and 4b).

[22] Compared with the TMPA data, the model overestimates precipitation in broad regions of the model domain, except over the Sea of Japan (East Sea) between the Korean peninsula and Japan (Figure 5a). There are cyclonic circulation anomalies in southern Japan which are associated with excessive precipitation. A low-level divergent flow over the Sea of Japan (East Sea) is associated with the underestimated amount of precipitation. Cyclonic flows circulation to the south of Korea and Japan is associated with convergence of the low-level wind over the excessive precipitation areas. In relation to overall weakening of sea level pressure and strengthening of precipitation, there exist warm biases in the southern part of the model domain and cold biases in the north (Figures 5b, 5c). A small area of cold biases in southeastern Japan and southern Korea in Figure 5b can be related to overestimated precipitation, which reduces the downward solar radiation due to enhanced cloudiness. It might also be possible that moisture reaching this area at 850 hPa cools the air. It is shown that cyclonic circulations appear over the whole domain at the upper troposphere compared to the FNL data (Figure 5c). The CTL experiment simulates the overall pattern of 500 hPa height fields reasonably (not shown), but the values are higher than those from the FNL data (Figure 5d).

[23] Overall, the CTL run reproduces the typical monsoonal circulation features and associated precipitation over East Asia in summer, even though discernable biases are produced. Excessive precipitation accompanying weakened surface pressures appeared over the oceans. The impact of the inclusion of air-sea interaction on these biases will be discussed below.

3.2. Impact of Individual Components in Air-Sea Interaction (July 2006)

3.2.1. Ocean Mixed Layer Model

[24] Figure 6 depicts the differences in monthly averaged SST between the CTL and OML experiments, together with the monthly averaged 10 m wind speed (m s^{-1}) from the OML experiment. It is seen that the monthly averaged values of differences in SST are relatively small. It is because in this study the SST and OML depth are initialized every 24 hours to add a modulated variation due to wind-driven mixing to daily SST value. In the case of *Davis et al.*, [2008] the SST is kept cooling during the model integration since the OML depth is initialized only at the model initial time. In this study, SST is nudged to the observed one every 24 hours since our purpose for coupling OML is to add dynamic effects of wind-driven mixing on the simulated climatology. However, the changes in upper-level circulations and sea-level pressure are not small since these are accumulated responses to the modulated SST during the 1 month period, as will be shown below.

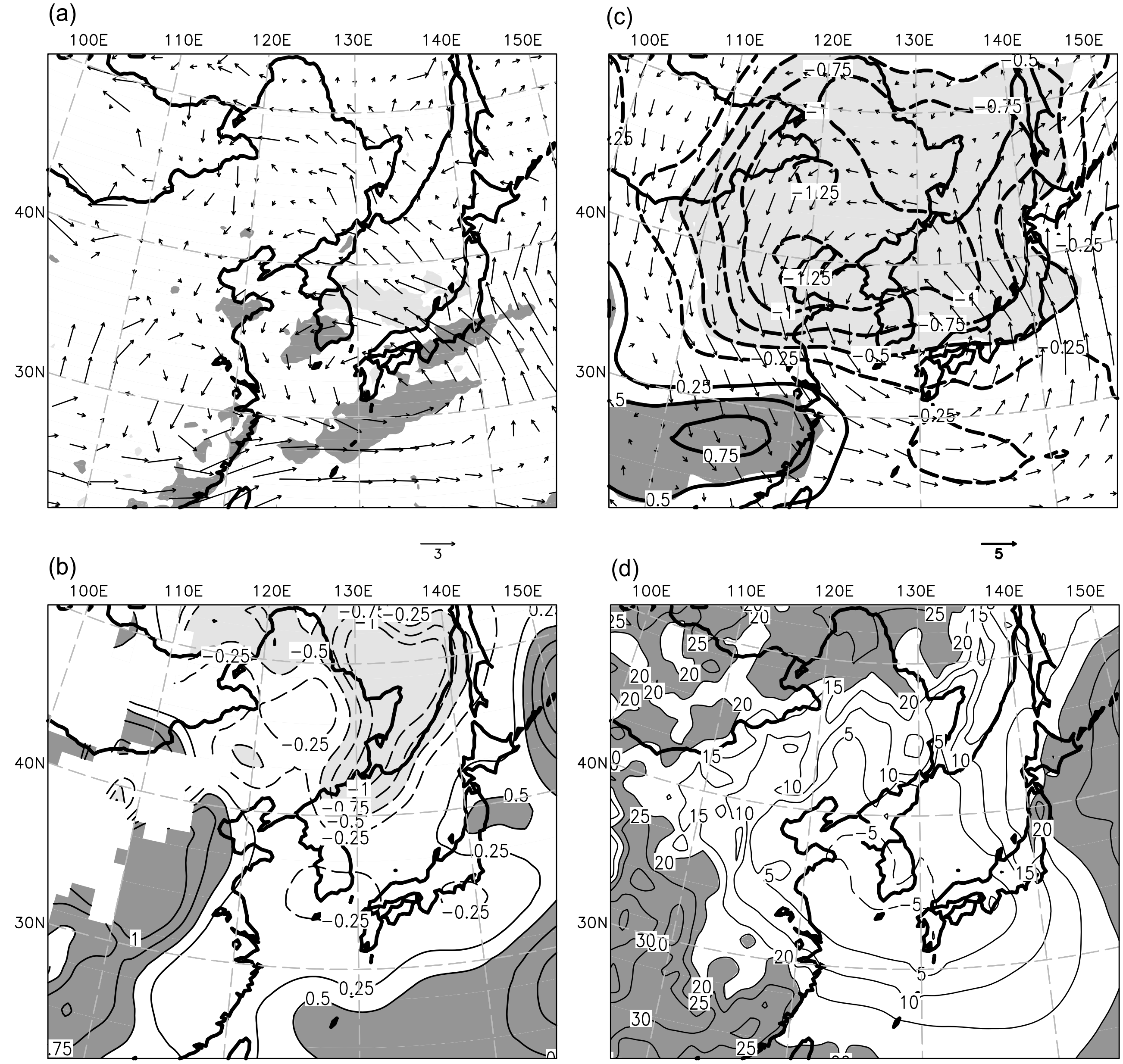

Figure 5. Differences in (a) monthly precipitation (mm) between the CTL and TMPA data (CTL minus TMPA, shaded), 850 hPa wind between the CTL and FNL data (CTL minus FNL, vector), and sea level pressure (CTL minus FNL, line), (b) 850 hPa temperature (K, line), (c) 500 hPa wind (vector) and temperature (K, line), and (d) 500 hPa geopotential height (m, line) in July 2006. In Figures 5a–d, solid lines are positive differences and dashed lines are negative differences. Dark shaded areas in Figures 5a–d indicate positive differences in precipitation (>200 mm), temperature (>0.5 K), temperature (>0.5 K), and geopotential height (>20 m), respectively, and light shaded areas in Figures 5a–d indicate the negative differences in precipitation (<−200 mm), temperature (<−0.5 K), temperature (<−0.5 K), and geopotential height (<−20 m), respectively.

[25] The impact of the ocean mixing on the simulated summer climate is shown in Figure 7. The OML experiment simulates higher sea level pressures over a broad area, covering the eastern China region to Japan, across the Korean peninsula, and including the adjacent oceans. Areas of increased pressure roughly coincide with the enhanced cooling (see Figures 6a and 7a). A region of lower sea level pressure appears over the northeastern part of the model domain, near Sakhalin, which seems to be an indirect effect. Westerly wind anomalies from the center of Korea to north of Japan would bring out the cyclonic anomaly in the north. At 850 hPa, the warming is centered in Korea, while in the

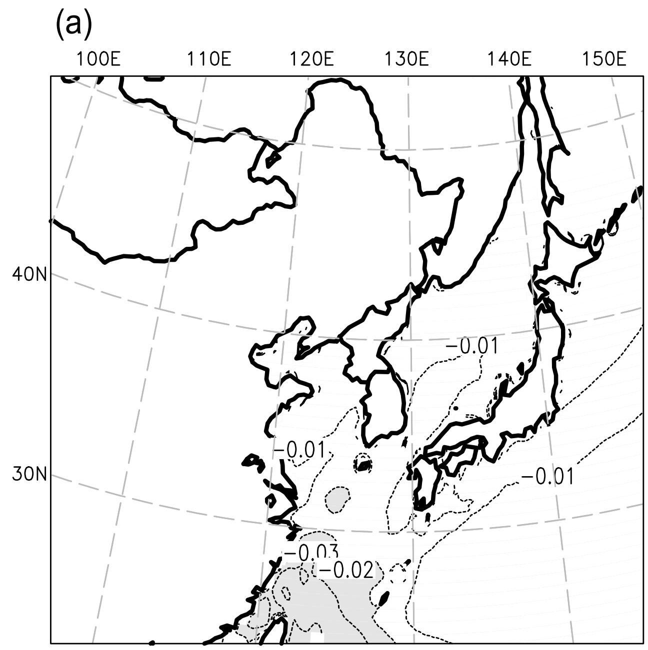

Figure 6. (a) Differences between the CTL and ocean mixed layer model (OML) experiments (OML minus CTL) in surface temperature (K) and (b) 10 m wind speed in the OML experiment (m s^{-1}) over the oceanic region in July 2006. Solid lines in Figure 6b indicate positive differences and dotted lines in Figure 6a indicate negative differences. Shaded areas in Figure 6a indicate differences in temperature >0.02 K and in Figure 6b indicate wind speed >4 m s^{-1}.

north of Korea it occurs at 500 hPa (Figures 7b, 7c). It is seen that the anticyclonic circulation anomalies centered over the Korean peninsula at 850 hPa extend up to 500 hPa (Figure 7c). The increase of the geopotential height at 500 hPa manifests the effects of SST changes on the monsoonal circulation in the upper atmosphere (Figure 7d).

[26] The precipitation amount is decreased (increased) where the sea level pressure is strengthened (weakened). The reason that the precipitation amount is reduced where the strengthened subtropical high appears is that cooling effects over the ocean's surface due to the wind-driven mixing increase stability. In turn, the stabilized condition over the ocean suppresses upward motion at the ocean's surface, which results in reduced precipitation. Consequently, the biases with weak pressure and excessive precipitation in the CTL run are alleviated by the OML experiment (Table 1). The decrease of the PBL height reflects a stable condition over the ocean due to the SST cooling (see Table 2). The warming effect in the upper layers over eastern China, Korea, and Japan seems to be due to a countering effect of a cloud-radiation interaction produced by a strengthened subtropical high in the south (see Figures 7b, 7c). The strengthened surface pressure accompanying the reduction of precipitation results in an increase of solar insolation (see also Table 2). In addition, it is shown that although the monthly averaged cooling rate of SST is small (see Figure 6a), the magnitude of the strengthened subtropical high is large. This is because the cooled SST not only causes the local changes, but also seems to have a dynamical link in monsoonal circulation. The increased stability induced by cooled SST strengthens the subtropical high and weakens the monsoonal rain band as mentioned earlier. However, the strengthened anticyclonic winds over the Pacific (see Figure 7a) also prevent the moisture transport from the southeastern to northeastern part of Korea and Japan. Therefore, although the cooling rate of the SST is small, its influence on the large-scale can be relatively significant.

[27] The results with a thicker initial mixed layer depth of 50 m exhibited a similar pattern to those from the OML experiment in terms of pressure and precipitation, but the effects were smaller in terms of the magnitude difference in the subtropical high (not shown). This is because the cooling rate due to the deeper initial mixed layer depth is smaller than that of the thinner mixed layer depth. Therefore, it can be said that reducing the initial mixed layer depth is useful to reflect the impact of the ocean mixed layer when SSTs are updated.

[28] From the analyses of time series data (not shown), it was found that the effects of sea level pressure and upper layer values are not directly influenced by SST variation, whereas other surface variables (e.g., SST, surface heat flux) responded directly to the wind-driven cooling. These analyses manifest a dynamical link between the monsoonal-circulation and the local effects of cooled SST.

3.2.2. Prognostic Sea Surface Skin Temperature Scheme

[29] Figure 8 exhibits the differences in monthly averaged SST over the ocean between the CTL and TDI experiments, along with the downward solar radiation from the TDI

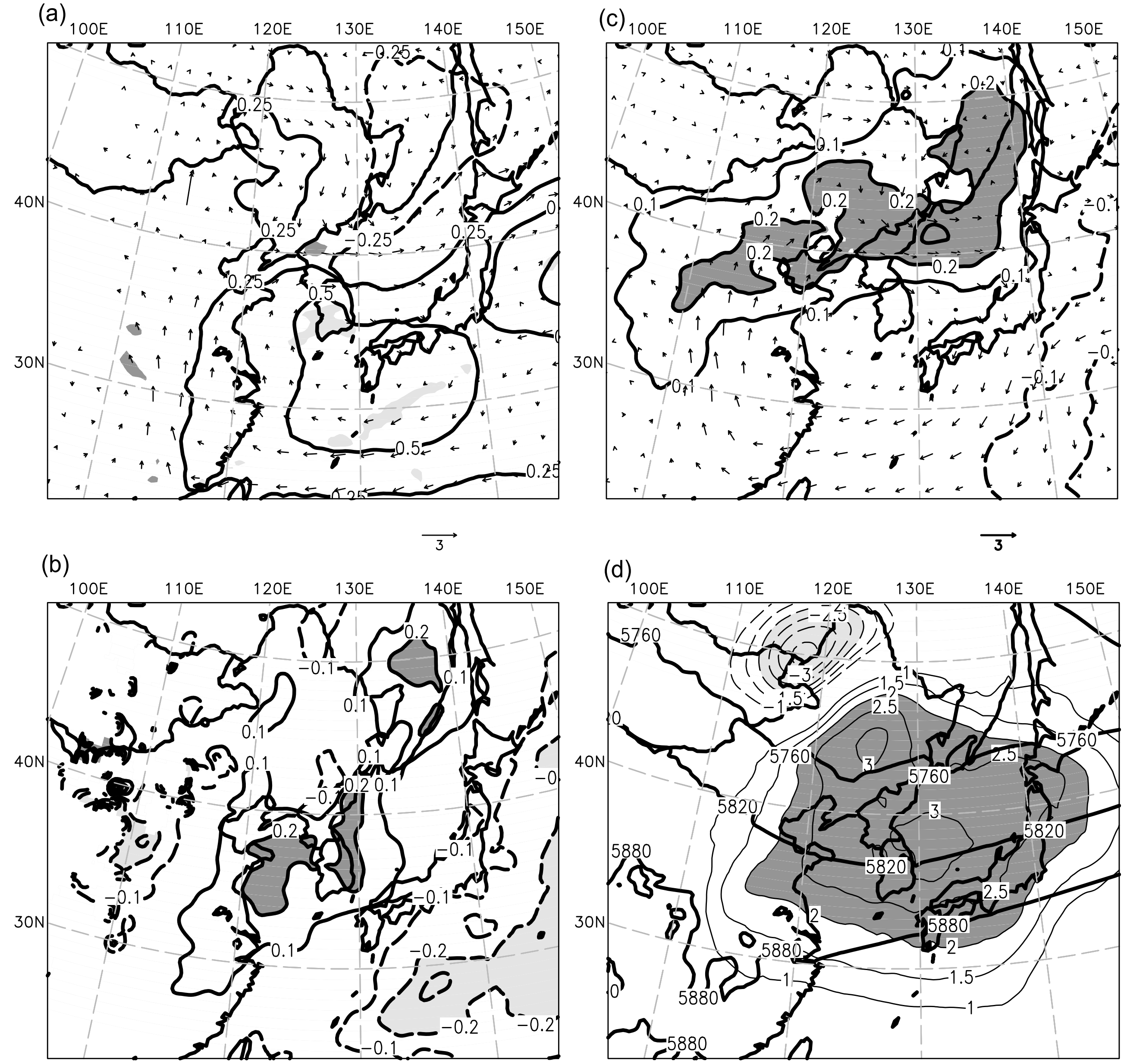

Figure 7. Differences between the CTL and the OML experiments (OML minus CTL) in (a) sea level pressure (mb, line), 850 hPa wind (vector), precipitation (mm, shaded), (b) 850 hPa temperature (K, line), (c) 500 hPa wind (vector) and temperature (K, line), and (d) 500 hPa geopotential height (m, line) in July 2006. In Figures 7a–d, solid lines are positive differences and dashed lines are negative differences. Dark shaded areas in Figures 7a–d indicate positive differences in precipitation (>100 mm), temperature (>0.2 K), temperature (>0.2 K) and geopotential height (>2 m), respectively, and light shaded areas in Figures 7a–d indicate negative differences in precipitation (<−100 mm), temperature (<−0.2 K), temperature (<−0.2 K), and geopotential height (<−2 m), respectively.

experiment. Figure 8 represents a tendency of SST warming due to the solar heating during the daytime. By and large, impacts on the simulated climate due to the inclusion of diurnal variation of SST are opposite to those from the OML experiment (see Figures 7 and 9). Compared to the CTL experiment, the TDI experiment tends to weaken pressures over the region from southeastern China to Japan and across the Korean peninsula, including the adjacent areas (Figure 9a). The increase of pressures is evident to the northwest of the negative anomaly region. The amount of precipitation is increased (decreased) where the sea level pressure is weakened (strengthened), as for the OML experiment. The increase of cyclonic rotation centered south of the Korean peninsula is evident where precipitation is

Table 1. One Month Averaged Sea Level Pressure and Precipitation in Each Experiment

Experiment[a]	Sea level Pressure (hPa)			Precipitation[b] (mm d^{-1})		
	Ocean	Land	Whole Domain	Ocean	Land	Whole Domain
CTL	1008.4	1003.6	1006.1	7.98 (6.11)	7.43 (5.42)	7.73 (5.79)
OML	1008.6	1003.7	1006.3	7.51 (5.66)	7.59 (5.51)	7.55 (5.59)
TDI	1008.2	1003.7	1006.1	8.03 (6.11)	7.43 (5.45)	7.75 (5.80)
DRG	1008.8	1004.0	1006.5	6.83 (5.00)	7.46 (5.38)	7.12 (5.18)
ALL	1008.8	1004.0	1006.5	6.84 (5.04)	7.42 (5.34)	7.11 (5.19)
OBS	1009.0	1004.3	1006.9	4.74	5.65	5.14

[a]CTL = control; OML = ocean mixed layer effects; TDI = sea surface skin temperature effects; DRG = revised roughness length effects; ALL = all three components (ocean mixed layer, sea surface skin temperature, and revised roughness length effects); OBS = observations.
[b]Precipitation values in parentheses indicate convective rain.

increased. At 850 hPa, a relative cooling is centered over the northern Yellow Sea and a warming in northeastern Mongolia (110°E–20°E, 48°N–53°N) (Figure 9b). At 500 hPa, cooling is pronounced in eastern Manchuria with accompanying northeasterly wind anomalies (Figure 9c). These changes in wind and temperature in the lower troposphere bring about the reduction of geopotential height at 500 hPa over a broad area covering eastern China, Korea, Japan, and adjacent oceans (Figure 9d). The increase of the height in eastern Mongolia reflects warming at 850 hPa.

[30] The increased surface temperature over the ocean from solar heating induces increase in latent heat fluxes and PBL height (Table 2), forming unstable conditions near the surface, as compared to the CTL experiment. In turn, these unstable conditions strengthen the upward motion over the surface and result in weakening of the subtropical high, which induces the enhanced precipitation centered over the oceans south of the Korean peninsula. Accompanying the reduction of precipitation over land, the increase of pressure to the northwest of the subtropical high can be attributed to the weakened moisture transport in the lower troposphere along the western periphery of the subtropical high. As in the opposite response to the ocean mixed layer, the weakened surface pressure over the ocean accompanying the reduction of precipitation results in cooling in the upper layers due to the increase of cloudiness.

[31] The warming of SST in the TDI experiment is larger than its cooling rate in the OML experiment. However, the magnitudes of changed sea level pressure and precipitation are smaller than those of the OML experiment (see Table 1). Therefore, it can be inferred that dynamical feedback effects are small on monsoonal circulation compared to the case of SST cooling.

3.2.3. Revised Roughness Length Formulation

[32] It is apparent that roughness length has a relatively large effect on the simulated climate, as shown in Figure 10a and Table 1. A broad area of positive anomalies for surface pressure is evident, centered over the subtropical high region and accompanying the overall reduction of precipitation in large areas of the oceans. The northern Pacific high is strengthened significantly by more than 1 hPa near the center. At 850 hPa, cooling is dominant in all areas except northeastern Mongolia (Figure 10b). At 500 hPa, a warming associated with anticyclonic circulation anomalies is observed in eastern Siberia and northern Manchuria (100°E–125°E, 30°N–50°N) (Figure 10c). Cooling at 500 hPa appears over the oceanic area and the northeastern part of Korea. The 500 hPa geopotential is generally higher west of 130°E and lower to the east (Figure 10d).

[33] The immediate effect of the revised roughness length is the reduction of surface fluxes through the smaller exchange coefficient, as compared to the Charnock formula. The total amount of surface flux decreases to 93.6 W m^{-2} in the DRG experiment from 106.5 W m^{-2} in the CTL experiment (Table 2). The relatively dominant effect compared with the previous sensitivity experiments can be attributed to the heat exchange coefficient, which directly changes the surface flux. The reduced C_d due to the decreased roughness length can also increase the surface wind through reduced momentum mixing, which can increase the surface flux; however, the reduction of C_h played a dominant role in reducing the amount of flux. A slight increase of sensible heat flux can be attributed to the increase of surface wind, but its effect is negligible. In total, decreased roughness length directly reduces the latent heat flux; hence, strong stability appears and the subtropical high is strengthened over the ocean's surface. In turn, the amount

Table 2. One Month Averaged Latent Heat Flux, Sensible Heat Flux, Downward Solar Radiation, and Planetary Boundary Layer Height Over the Ocean in Each Experiment

Experiment[a]	Latent Heat Flux (W m^{-2})	Sensible Heat Flux (W m^{-2})	Downward Solar Radiation (W m^{-2})	Planetary Boundary Layer Height (m)
CTL	103.9	2.6	263.4	409.5
OML	98.9	2.5	264.9	408.8
TDI	104.2	2.1	265.3	417.7
DRG	90.6	3.0	270.2	412.8
ALL	90.3	2.4	271.4	418.7

[a]CTL = control; OML = ocean mixed layer effects; TDI = sea surface skin temperature effects; DRG = revised roughness length effects; ALL = all three components (ocean mixed layer, sea surface skin temperature, and revised roughness length effects).

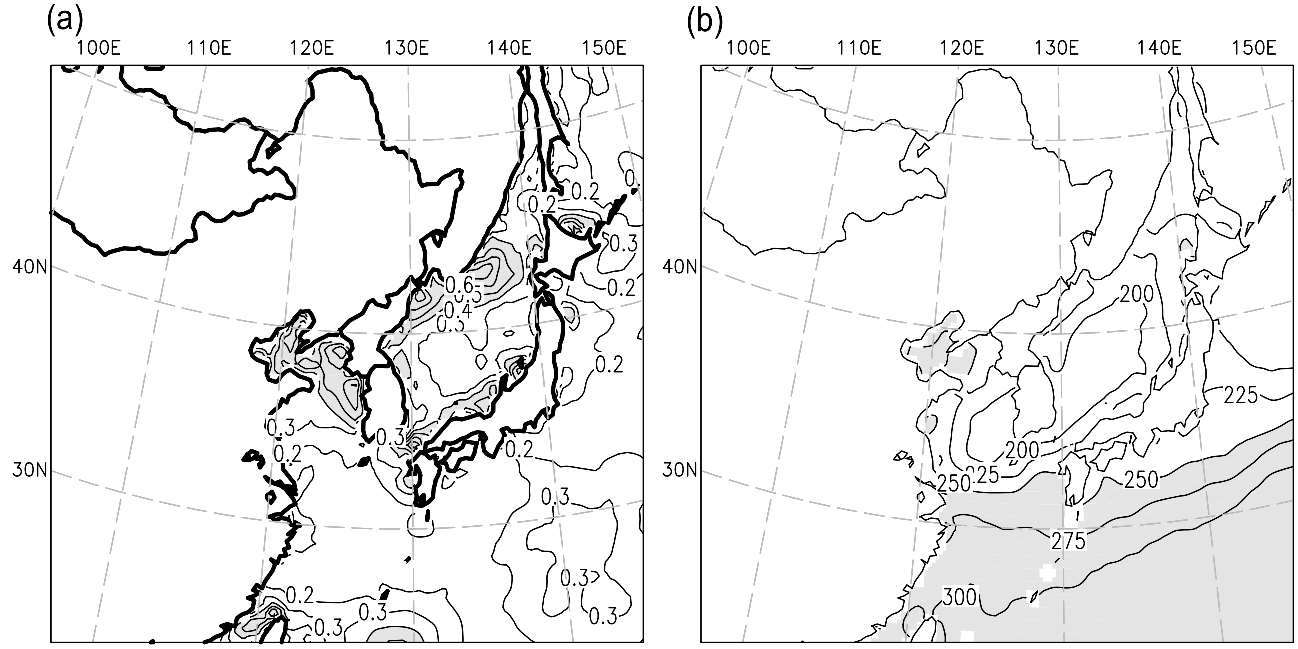

Figure 8. (a) Differences in surface temperature (K) over the oceanic region between the CTL and prognostic sea surface skin temperature scheme (TDI) experiments (TDI minus CTL) and (b) downward solar radiation (W m^{-2}) of the TDI experiment over the ocean in July 2006. Solid lines in Figure 8a indicate positive differences and dotted lines indicate negative differences. Shaded areas in Figure 8a indicate differences in surface temperature >0.4 K and in Figure 8b indicate downward solar radiation >250 W m^{-2}.

of precipitation is reduced by the strengthened subtropical high over the ocean. The decrease of convective precipitation is pronounced over the oceans compared to that over land (Table 1). This is due to the weakened surface fluxes, which in turn provide a less favorable sub-cloud environment for deep convection. Meanwhile, increased surface pressure can enhance solar heating, which warms the air column aloft.

[34] The overall effect, with the increased sea level pressure in the DRG run, is qualitatively in line with the mixed layer effect in the OML experiment. However, the cooling at 850 hPa is distinct, whereas more warming appears in the OML experiment (see Figures 7b and 10b). This indicates that the effect of the roughness length expands in the lower troposphere in the DRG experiment. This is because cooling due to the reduced roughness length overwhelms the warming due to stronger solar insolation caused by strengthened subtropical high. Therefore, it can be said that effects of the roughness length are greater than the countering effect of cloud-radiation interaction.

3.2.4. Combined Effects

[35] As examined in the previous sub-sections, the effect of the revised roughness length would be a pronounced factor on changes in precipitation and monsoonal circulations. The tabulated results in Table 1 reveal that the ALL experiment results are similar to those from the DRG experiment. This occurs because the ocean mixed layer effects largely cancel the diurnal variation of SST. A comparison of Figures 5a and 11a confirms that overall improvement is achieved when all three effects are taken into account. However, a close inspection reveals that the magnitude of the changes in precipitation and large-scale features improves compared to the magnitude changes from the DRG experiment (Figure 11b). The intensity of sea level pressure over Korea and Japan is further reduced toward the observations, although a negative effect is visible in Siberia with the increase of pressure. The reduction of precipitation over the Yellow Sea between China and Korea, and over southern Japan is a positive effect, even though the magnitude is small.

[36] Methods used in this study also affect typhoons that developed during the simulated period. In the case of Typhoon Bilis, the tracks and intensities reproduced in each experiment are improved compared to the CTL experiment (not shown). However, typhoons do not considerably effect monthly climate simulations. For monthly variation, the OML experiment tends to produce higher sea level pressure compared to the CTL simulation although typhoons do not exist over the ocean (Figure 12). These features appear in the DRG and ALL experiments. In addition, the TDI simulation produces lower sea level pressure under low wind conditions, which help the diurnal heating at surface (not shown). The big differences in sea level pressure between the CTL and the OML, DRG, and ALL experiments from 15 July to 22 July and from 29 July to 1 August are due to large differences in wind speed (not shown). Therefore, it can be said that the typhoons do not play a distinct role in the monthly climate.

[37] For the ALL simulation results, we can say that it is plausible to consider all three components since they are physically based. Therefore, a robust evaluation of air-sea interaction on a climate will be conducted by comparing the

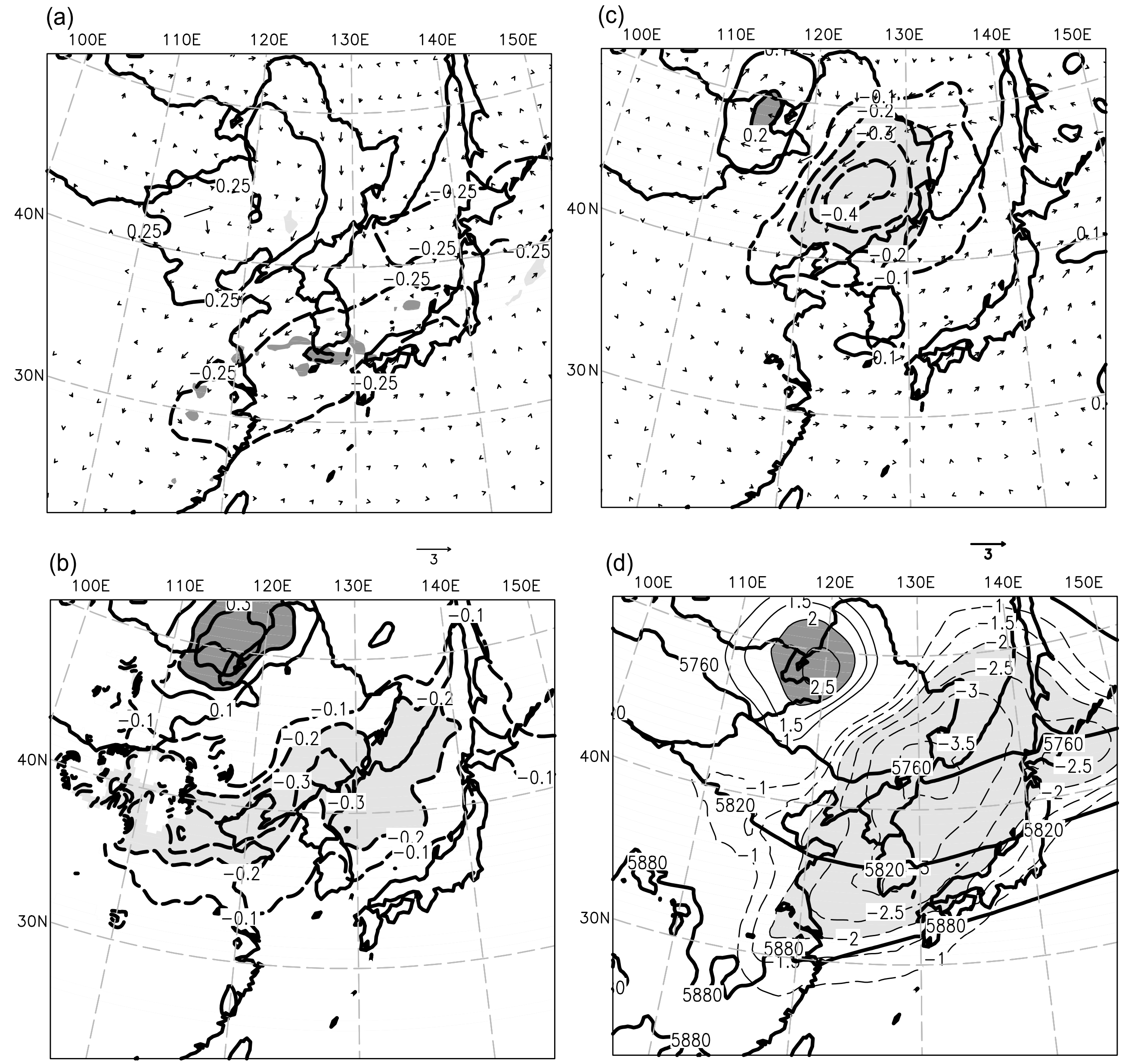

Figure 9. Differences between the CTL and TDI experiments (TDI minus CTL) in (a) sea level pressure (mb, line), 850 hPa wind (vector), precipitation (mm, shaded), (b) 850 hPa temperature (K, line), (c) 500 hPa wind (vector) and temperature (K, line), and (d) 500 hPa geopotential height (m, line) in July 2006. In Figures 9a–d, solid lines are positive differences and dashed lines are negative differences. Dark shaded areas in Figures 9a–d indicate positive differences in precipitation (>100 mm), temperature (>0.2 K), temperature (>0.2 K) and geopotential height (>2 m), respectively, and light shaded areas in Figures 9a–d indicate the negative differences in precipitation (<−100 mm), temperature (<−0.2 K), temperature (<−0.2 K), and geopotential height (<2 m), respectively.

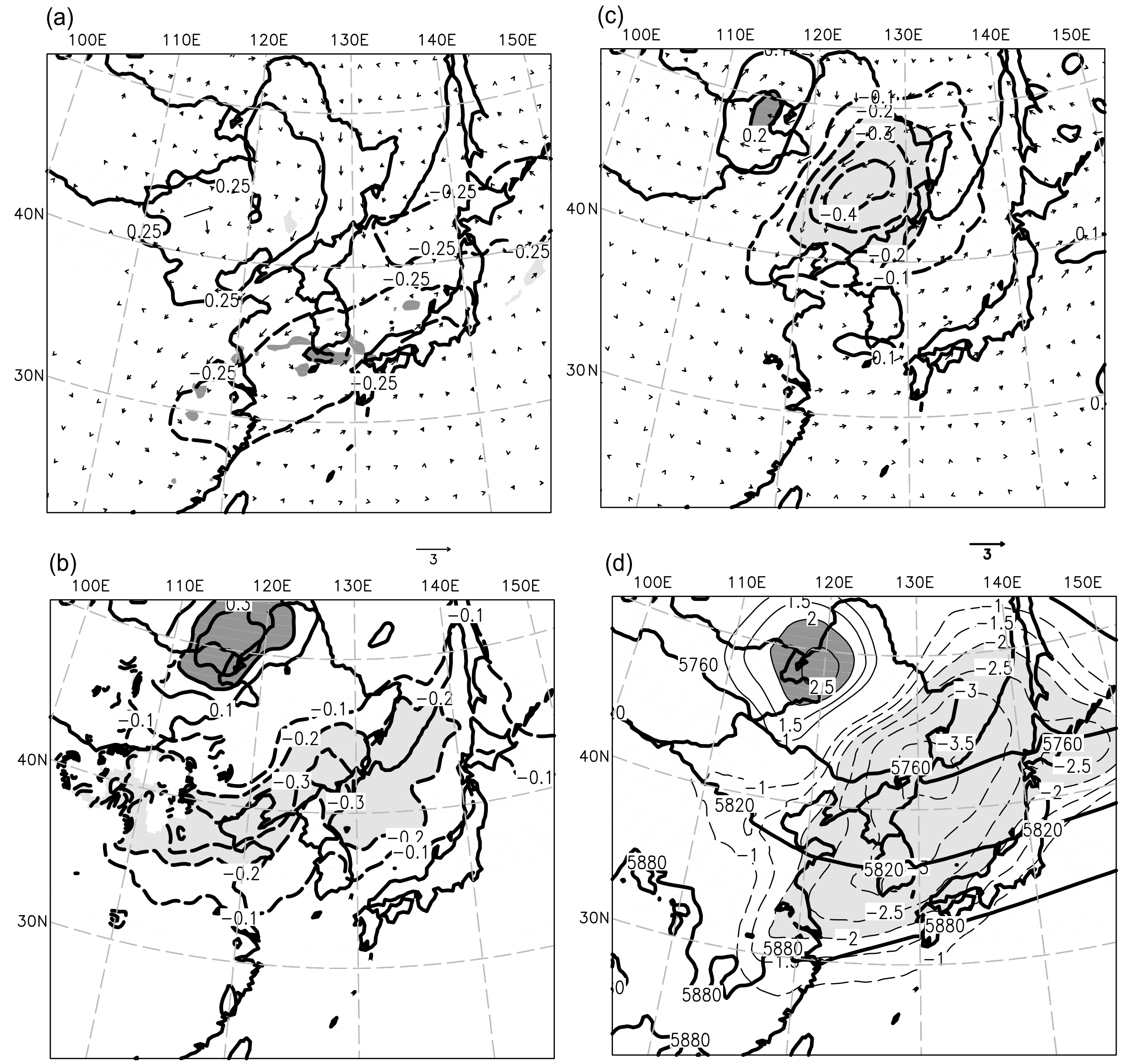

Figure 10. Differences between the CTL and revised roughness length formulation (DRG) experiments (DRG minus CTL) in (a) sea level pressure (mb, line), 850 hPa wind (vector), precipitation (mm, shaded), (b) 850 hPa temperature (K, line), (c) 500 hPa wind (vector) and temperature (K, line), and (d) 500 hPa geopotential height (m, line) in July 2006. In Figures 10a–d, solid lines are positive differences and dashed lines are negative differences. Dark shaded areas in Figure 10a–d indicate positive differences in precipitation (>100 mm), temperature (>0.4 K), temperature (>0.4 K), and geopotential height (>2 m), respectively, and light shaded areas in Figures 10a–d indicate the negative differences in precipitation (<−100 mm), temperature (<−0.4 K), temperature (<−0.4 K), and geopotential height (<2 m), respectively.

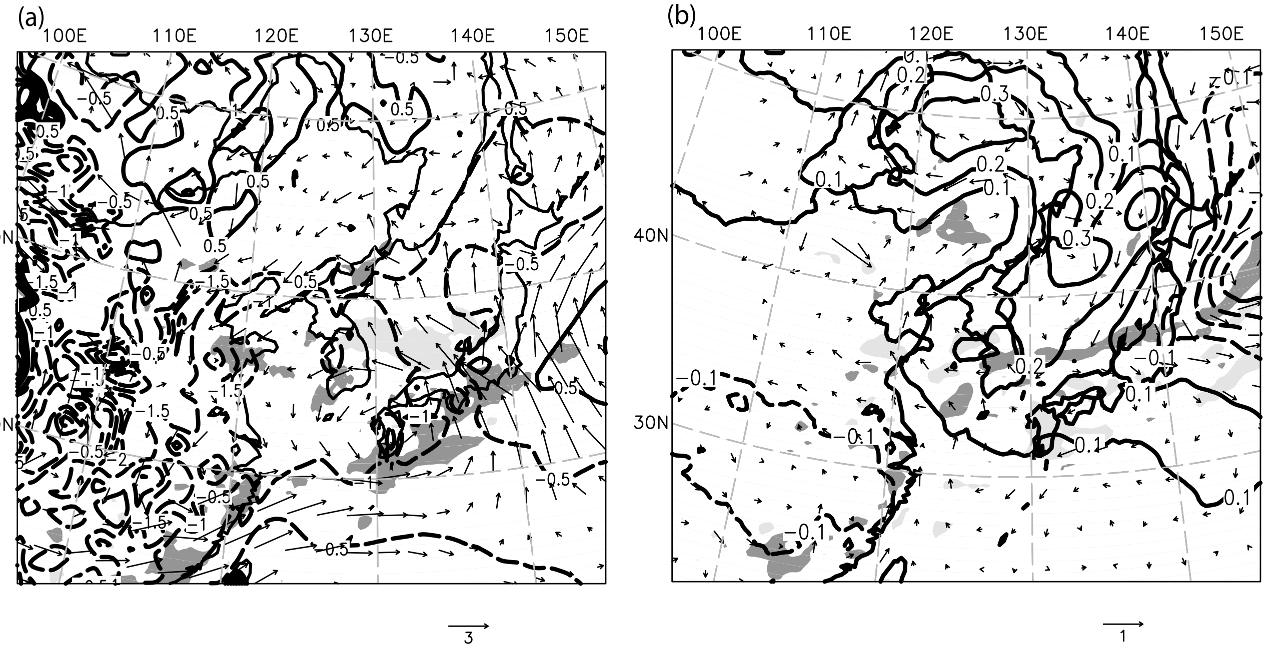

Figure 11. Differences in monthly averaged sea level pressure (mb, line), 850 hPa wind (vector), and 1 month accumulated precipitation (mm, shaded) (a) between the ALL (OML-TDI-DRG) experiment and observations, and (b) between the ALL and DRG experiments (ALL minus DRG). Dark shaded areas in Figures 11a and b indicate positive differences in precipitation (>200 mm) and precipitation (>50 mm), respectively, and light shaded areas in Figures 11a and b indicate the negative differences in precipitation (<−200 mm) and precipitation (<−50 mm), respectively.

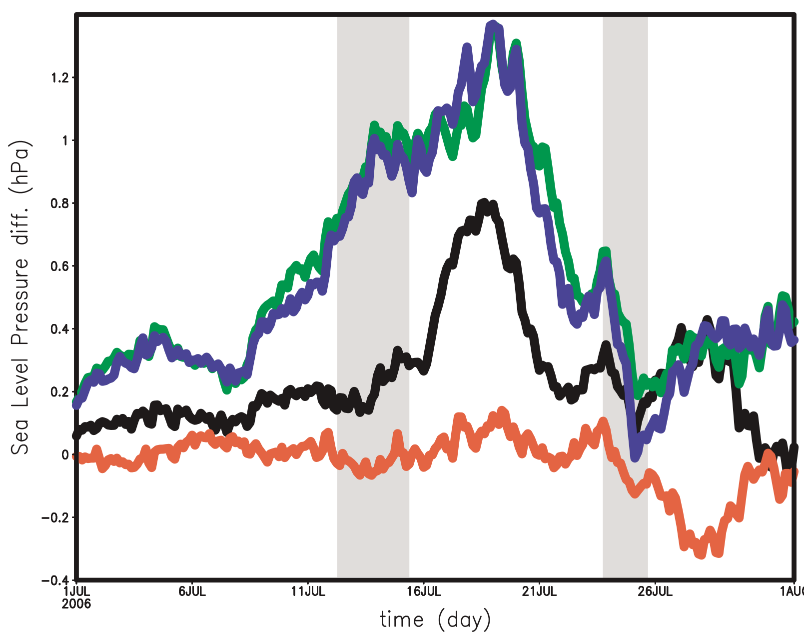

Figure 12. Time series of differences in sea level pressure (hPa) over the ocean between the CTL and OML (OML minus CTL, black line), CTL and TDI (TDI minus CTL, red line), CTL and DRG (DRG minus CTL, green line), and CTL and ALL (ALL minus CTL, blue line) experiments. Shaded areas indicate periods when typhoons Bilis and Kaemi were present in the model domain (0600 UTC 12 July to 0600 UTC 15 July for Typhoon Bilis and 0600 UTC 24 July to 1800 UTC 25 July for Typhoon Kaemi).

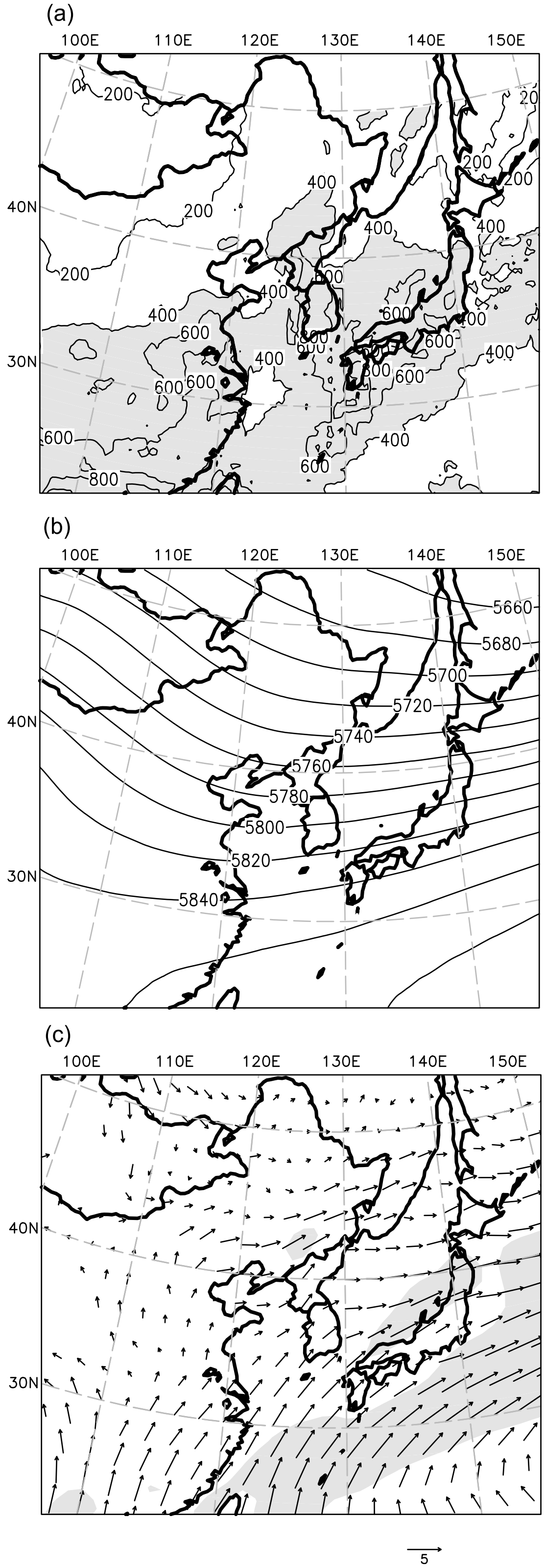

Figure 13. The 9-year (2000–2008) mean June–August (a) precipitation (mm) from the TMPA data, (b) 500 hPa geopotential height (m), and (c) 850 hPa wind (m s^{-1}) from the reanalysis data. Contour intervals are 200 mm in Figure 13a and 20 m in Figure 13b. Shaded areas in Figure 13a are >400 mm and in Figure 13c are >4 m s^{-1}.

results from the CTL and ALL experiments for a multi-year simulation, as discussed below.

3.3. Impacts of the Air-Sea Interaction Package on Simulated Climatology (2000–2008)

[38] In this section, results from 9-year-averaged summer simulations with the CTL and ALL packages are compared. The impacts of all three effects on the distribution of precipitation and large-scale features for the 9-year-averaged summers qualitatively follow those from the 1 month run discussed in section 3.2, as discussed below.

[39] The 9-year-averaged June–August precipitation for TMPA data represents the monsoonal rain band extending northeastward from southern China to the northern part of Japan (Figure 13a). The climatology of the geopotential height at 500 hPa shows the subtropical high over the northwestern Pacific and the midlatitude East Asian trough, elongated northeastward from east China to Manchuria (Figure 13b). Associated with the subtropical high, there are southerly or southwesterly winds at 850 hPa, which transport warm and moist air from the northwestern Pacific to Korea and Japan (Figure 13c).

[40] The simulated precipitation for summers (June–August) over a 9 year (2000–2008) period is shown in Figure 14. The CTL and ALL experiments reproduce the precipitation center over southern China, Korea, and Japan fairly well (Figures 14a, 14b). However, excessive precipitation over the sub-tropics and northern China is prominent in the case of the CTL run, whereas a deficit in the amount of precipitation occurs in the central region of the monsoon band, near Korea and Japan (Figure 14c). These bias patterns were identified in the 1 month simulation, but with weaker magnitudes (see Figure 5a). On the other hand, the ALL experiment tends to reduce the bias over the subtropical region, which is in the southern part of the domain, by reducing the precipitation amount (Figure 14d). A further reduction near the Korean peninsula causes the climatology to deteriorate, but the tabulated skills show that the overall skill for monsoonal precipitation in the ALL experiment is better than in the CTL run (Table 3).

[41] The simulated 500 hPa height fields agree fairly well with the FNL data, but with a discernible positive bias (Figures 15a, 15b). The CTL experiment overestimates the height by about 20–50 m, with the maximum elongating from southwest to northeast (Figure 15c). These biases are not changed by the effective air-sea interaction, but a slight reduction of the bias is visible (Figure 15d). This comparison proves that the large-scale features in the upper troposphere are not distinctly altered by the air-sea interaction. This could be partly due to the forced large-scale features within the RCM platform designed in this study.

[42] It is seen that the low-level jets from southeastern China to the northeastern Sea of Japan are well-represented in the CTL and ALL runs (Figures 16a, 16b). However, the anticyclonic circulation over the northwestern Pacific is underestimated in the CTL experiment (Figure 16c). These biases in cyclonic circulation weaken the subtropical high over the monsoon region, resulting in excessive precipitation. On the other hand, the ALL experiment enhances the anticyclonic circulation over the northwestern Pacific, as compared to the CTL run (Figure 16d). These changes in the

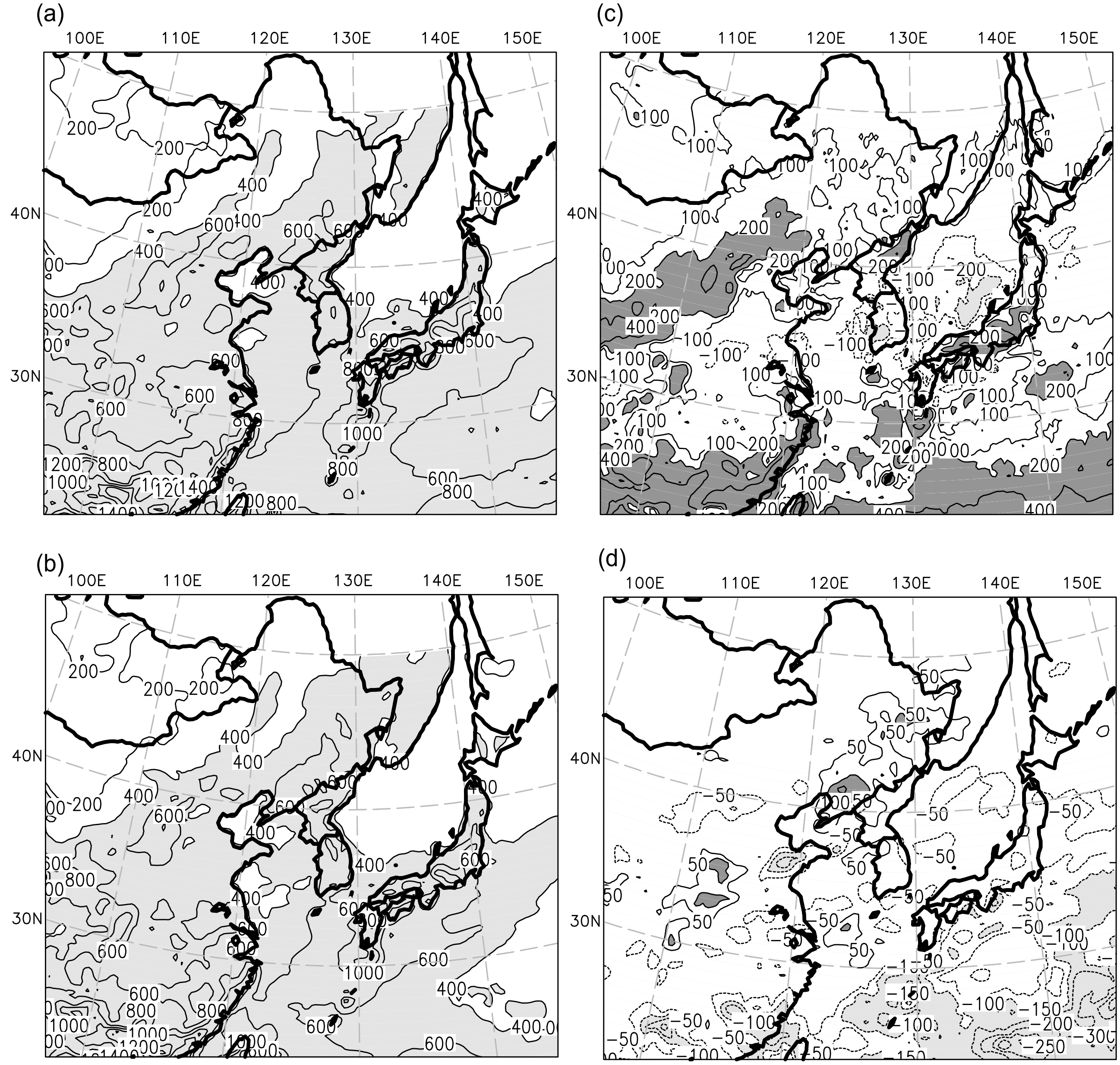

Figure 14. The 9-year (2000–2008) mean June–August precipitation (mm) for (a) CTL, (b) ALL, (c) the difference between CTL and the TMPA data (CTL minus TMPA), and (d) the difference between the ALL (combined ocean mixed layer, sea surface skin temperature, and revised roughness length effects) and CTL experiments (ALL minus CTL). Contour intervals are 200 mm in Figures 14a–c and 50 m in Figure 14d. Shaded areas are >400 mm in Figures 14a and b. Dark (light) shaded areas in Figure 14c denote that the model overestimates (underestimates) precipitation by >200 mm, and by >100 mm in Figure 14d.

lower tropospheric circulation play a role in reducing the excessive oceanic precipitation in the case of the CTL run (see Table 3).

[43] Figure 17 compares the inter-annual variation of seasonal precipitation for 9 years in the CTL and ALL experiments, and for the whole domain, land, and ocean obtained from the TMPA observation. The TMPA data over the whole domain present a maximum in 2000 and a minimum in 2004 (Figure 17a). The CTL experiment reproduces the general trend of observed precipitation,

Table 3. Nine-Year (2000–2008) Mean June–August Bias, RMS Errors, and Pattern Correlation for the Simulated Precipitation Averaged Over Land, Ocean, and the Whole Domain[a]

	Jun–Aug Bias (mm d^{-1})		RMS Errors (mm d^{-1})		Pattern Correlation	
	CTL	ALL	CTL	ALL	CTL	ALL
Domain	1.94	1.12	3.08	2.11	0.71	0.78
Land	1.59	1.34	2.36	2.04	0.86	0.86
Ocean	2.25	0.92	3.57	2.12	0.50	0.66

[a]CTL = control; ALL = all three components (ocean mixed layer, sea surface skin temperature, and revised roughness length effects).

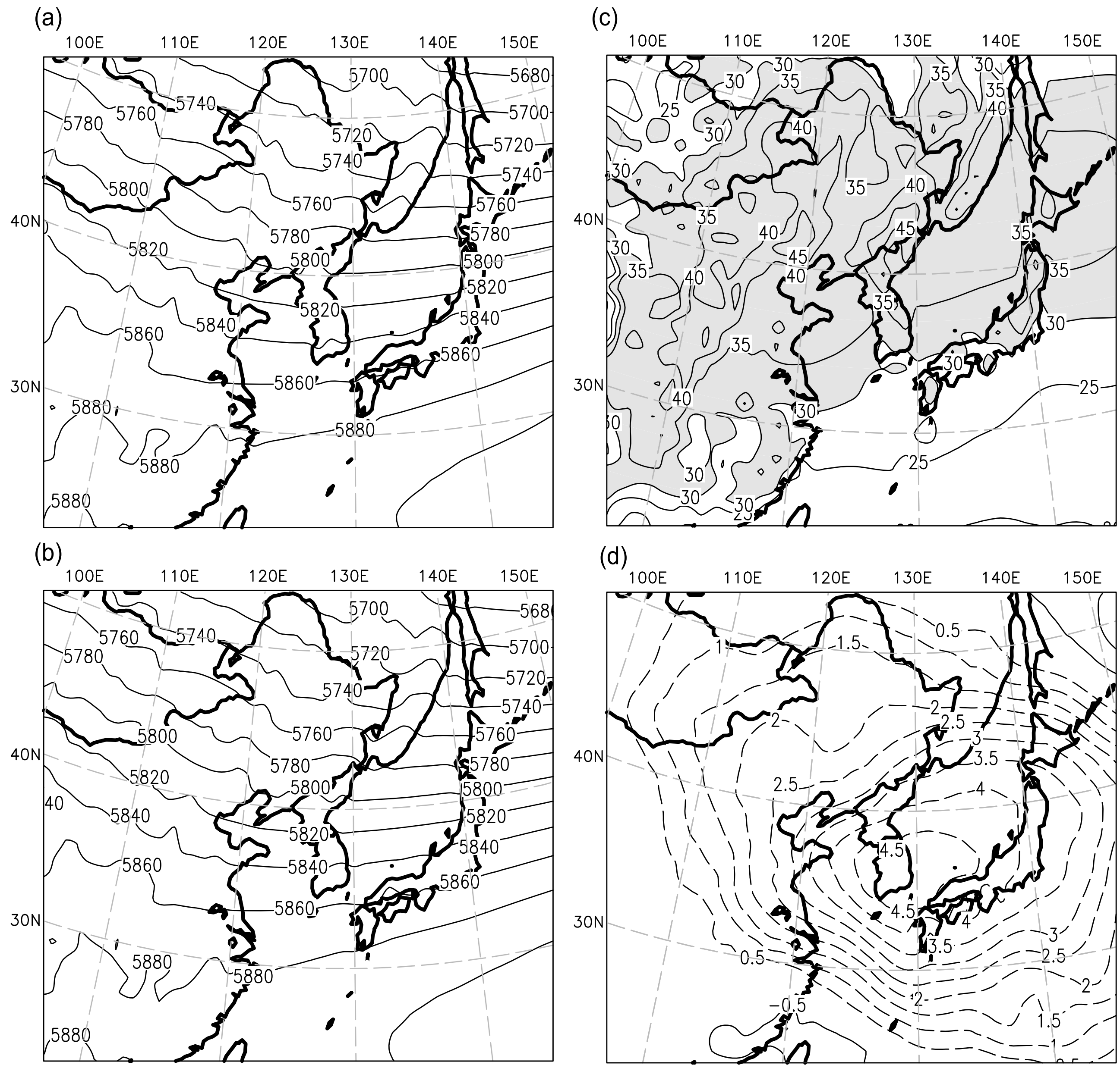

Figure 15. The 9-year (2000–2008) mean June–August 500 hPa geopotential height (m) for (a) CTL, (b) ALL, (c) the difference between CTL and FNL data (CTL minus FNL), and (d) the difference between ALL and CTL experiments (ALL minus CTL). Contour intervals are 20 m in Figures 15a and b, 5 m in Figure 15c, and 0.5 m in Figure 15d. Shaded areas in Figures 15c and d denote that the models overestimate by >30 m.

but generally overestimates the amounts. Meanwhile, it is clear that the ALL experiment reduces the amount of precipitation toward that which was observed, although a distinct underestimation is shown in 2001. Over land, the variations of the precipitation from the two runs show a trend similar to that seen in the observations, except for 2001 in the ALL experiment (Figure 17b). Over the oceanic region, both experiments have similar precipitation tendencies, but with a reduced bias (Figure 17c). From these results, it can be said that the inclusion of the air-sea interaction designed in this study effectively reduces the existing biases over the oceans, improving monsoon climatology.

4. Concluding Remarks

[44] The effect of air-sea interaction on the EASM is investigated using the WRF model. A series of sensitivity experiments related to air-sea interaction are executed with large-scale forcing from the NCEP FNL data. Three components for air-sea interaction, an ocean mixed layer model, the diurnal variation due to surface energy budget on the

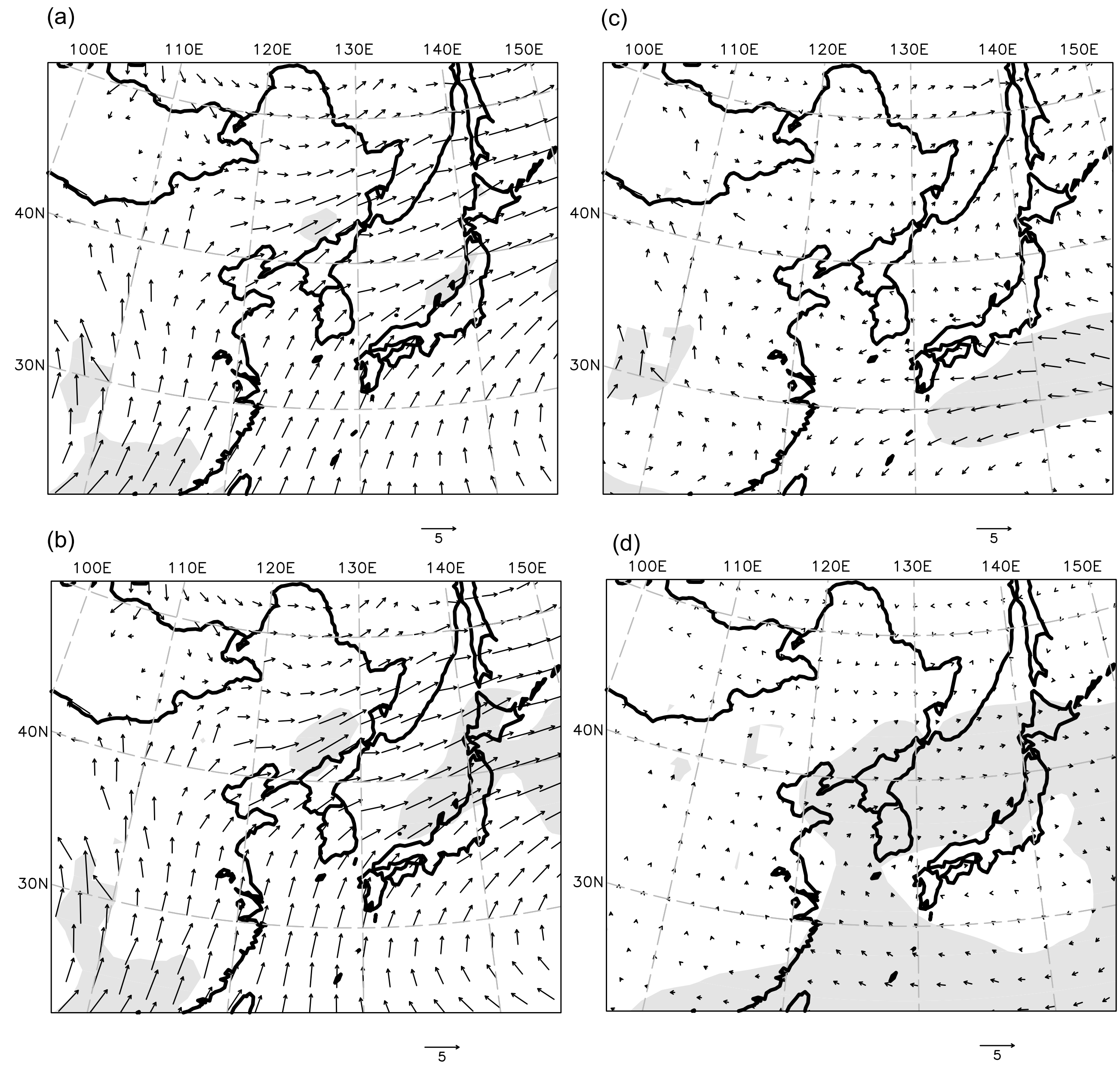

Figure 16. The 9-year (2000–2008) mean June–August 850 hPa wind (m s^{-1}) for (a) CTL, (b) ALL, (c) the difference between CTL and FNL data (CTL minus FNL), and (d) the difference between ALL and CTL experiments (ALL minus CTL). Shaded areas in Figures 16a and b denote that the wind speeds are >4 m s^{-1} and in Figures 16c and d denote that the models overestimate by >2 m s^{-1}.

SST, and a revised roughness length formula over water, are individually examined for July 2006. The impact of the combined components on the simulated seasonal summer climatology is further evaluated for 2000–2008.

[45] It is found that including the ocean mixed layer model cools the temperature at the water surface, stabilizing the thermodynamic structure near the surface. The resultant SST cooling reduces precipitation by increasing the surface pressure. A countering effect appears in the upper atmosphere by warming the air aloft because reduced cloudiness due to the stabilized condition enhances solar insolation over the ocean's surface. This in turn makes the overall impact on upper atmospheric circulation insignificant. The effect of the diurnal variation of SST, when considering the surface heat budget on the simulated monsoon, is opposite. Ocean surface warming, due to downward solar radiation during the daytime, overwhelms the cooling from outgoing longwave radiation. Thus, the overall impact includes enhanced precipitation activity within the unstable near-surface structure. Changes in the upper atmosphere above the boundary layer are not significant due to cloud-induced cooling. Replacing the Charnock formula for surface roughness length over water with the revised formula of *Donelan et al.* [2004] increases the surface pressure significantly by reducing the exchange coefficients. Precipitation reduction is also relatively pronounced. This effect is predominant when the three components are considered

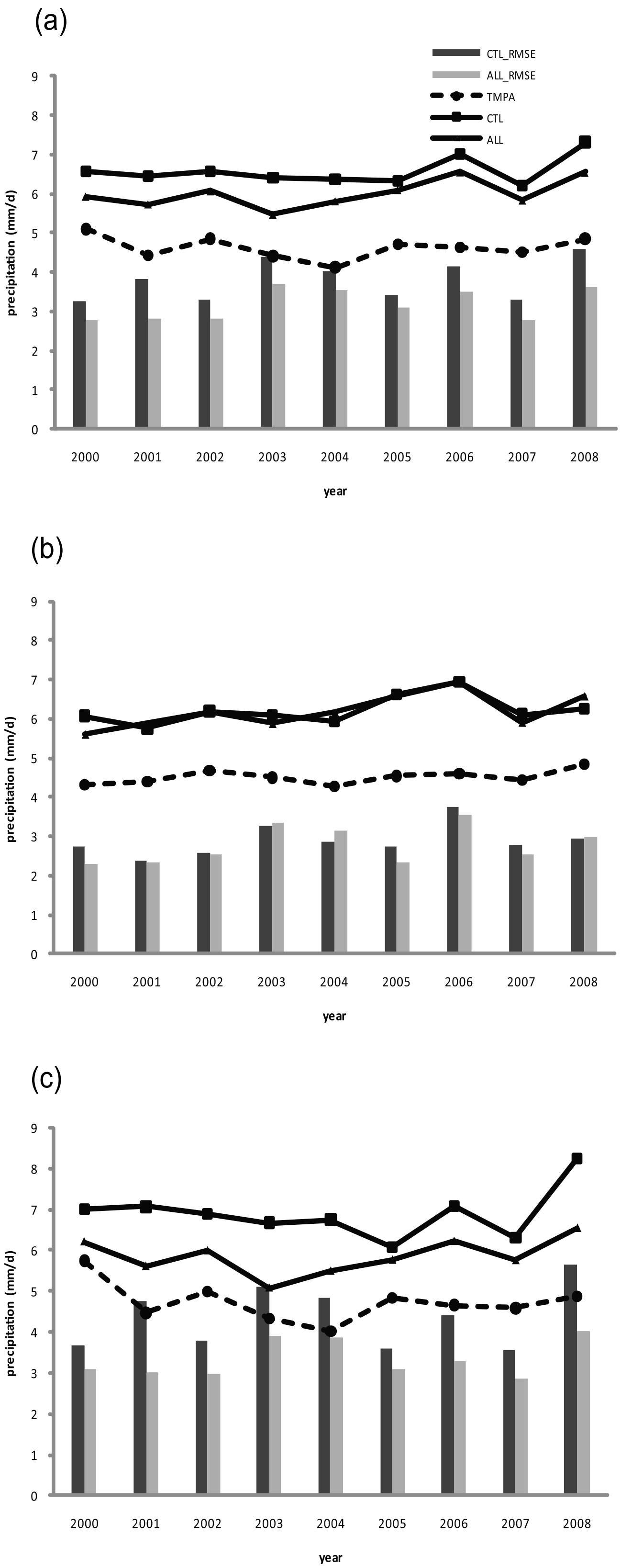

Figure 17. The 9-year (2000–2008) mean June–August precipitation rate (mm d^{-1}) and the RMS error (mm d^{-1}) from 2000 to 2008 over (a) the whole domain, (b) land, and (c) ocean, from TMPA data and from the CTL and ALL experiments.

together, since the mixed layer effect and diurnal SST effect largely cancel each other.

[46] It is evident that the effects of the air-sea interaction package, when employing the three components together, tend to improve the summer climate simulations over East Asia during 2000–2008. The overestimation of the simulated summer precipitation climatology without considering the air-sea interaction over the oceans is significantly alleviated. The weakening of the sub-tropical high is also improved. The inter-annual variability of the seasonal precipitation is realistic when the air-sea interaction is included.

[47] We understand that a regional-coupled ocean-atmosphere model system [e.g., *Döscher et al.*, 2002; *Seo et al.*, 2007; *Xie et al.*, 2007] is an ultimate resolution of the air-sea interaction issue, as in the GCM framework, but it is still not practical. The incorporation of a regional ocean model is computationally demanding, and the initial condition for ocean is not easy to obtain at a particular time. The results produced in this study suggest that this kind of modification to the surface layer module can be an effective way to reflect the air-sea interaction in the RCM framework, which is forced by the global model results. Since the SST from the global model results is a snapshot, our method can be useful in modeling the diurnal variation of SST. It is also true that all of the methods proposed in this study can be applied to numerical weather prediction models, not only for short-term range forecasting, but also for long-term simulation.

[48] **Acknowledgments.** This work was funded by the Korea Meteorological Administration Research and Development Program under Grant CATER_2007_4406. This work was supported by grant No. KSC 2009-G2-0002 from Korea Institute of Science and Technology Information (KISTI). The use of the computing system of the Supercomputing Center is also greatly appreciated.

References

Bao, J.-W., J. M. Wilczak, J.-K. Choi, and L. H. Kantha (2000), Numerical simulations of air-sea interaction under high wind conditions using a coupled model: A study of hurricane development, *Mon. Weather Rev.*, *128*, 2190–2210.

Carlson, T. N., and F. E. Boland (1978), Analysis of urban-rural canopy using a surface heat flux/temperature model, *J. Appl. Meteorol.*, *17*, 998–1013, doi:10.1175/1520-0450(1978)017<0998:AOURCU>2.0.CO;2.

Charnock, H. (1955), Wind stress on a water surface, *Q. J. R. Meteorol. Soc.*, *81*, 639–640.

Cherniawsky, J. W., and J. M. Oberhuber (1996), The seasonal cycle of mixed layer temperatures in a global ocean general circulation model, *Clim. Dyn.*, *12*, 171–183.

Chen, F., and J. Dudhia (2001), Coupling an advanced land-surface/hydrology model with the Penn State-NCAR MM5 modeling system. Part I: Model implementation and sensitivity, *Mon. Weather Rev.*, *129*, 569–585.

Dai, A., and K. E. Trenberth (2004), The diurnal cycle and its depiction in the community climate system model, *J. Clim.*, *17*, 930–951, doi:10.1175/1520-0442(2004)017<0930:TDCAID>2.0.CO;2.

Davis, C., et al. (2008), Prediction of landfalling hurricanes with the advanced hurricane WRF model, *Mon. Weather Rev.*, *136*, 1990–2005.

De Szoeke, R. A. (1980), On the effects of horizontal variability of wind stress on the dynamics of the ocean mixed layer, *J. Phys. Oceanogr.*, *10*, 1439–1454.

Donelan, M. A., B. K. Haus, N. Reul, W. J. Plant, M. Stiassine, H. C. Graber, O. B. Brown, and E. S. Saltzman (2004), On the limiting aerodynamic roughness of the ocean in very strong winds, *Geophys. Res. Lett.*, *31*, L18306, doi:10.1029/2004GL019460.

Dudhia, J. (1989), Numerical study of convection observed during the winter monsoon experiment using a mesoscale two-dimensional model, *J. Atmos. Sci.*, *46*, 3077–3107.

Döscher, R., U. Willén, C. Jones, A. Rutgersson, H. E. N. Meier, U. Hansson, and L. P. Graham (2002), The development of the coupled regional ocean-atmosphere model RCAO, *Boreal Env. Res.*, *7*, 183–192.
Emanuel, K. A., C. DesAutels, C. Hollway, and R. Korty (2003), Environmental control of tropical cyclone intensity, *J. Atmos. Sci.*, *61*, 843–858.
Fairall, C. W., E. F. Bradley, D. P. Rogers, J. B. Edson, and G. S. Young (1996a), Bulk parameterization of air-sea fluxes for tropical ocean-Global Atmosphere Coupled-Ocean Atmosphere Response Experiment, *J. Geophys. Res.*, *101*, 3747–3764, doi:10.1029/95JC03205.
Fairall, C. W., E. F. Bradley, J. S. Godfrey, G. A. Wick, J. B. Edson, and G. S. Young (1996b), Cool-skin and warm-layer effects on sea surface temperature, *J. Geophys. Res.*, *101*, 1295–1308, doi:10.1029/95JC03190.
Hong, S.-Y., J. Dudhia, and S.-H. Chen (2004), A revised approach to ice-microphysical processes for the bulk parameterization of cloud and precipitation, *Mon. Weather Rev.*, *132*, 103–120.
Hong, S.-Y., Y. Noh, and J. Dudhia (2006), A new vertical diffusion package with an explicit treatment of entrainment processes, *Mon. Weather Rev.*, *134*, 2318–2341.
Huffman, G., R. F. Adler, D. T. Bolvin, G. Gu, E. J. Nelkin, K. P. Bowman, Y. Hong, E. F. Stocker, and D. B. Wolff (2007), The TRMM multi-satellite precipitation analysis: Quasi-global, multi-year, combined-sensor precipitation estimates at fine scale, *J. Hydrometeorol.*, *8*, 38–55, doi:10.1175/JHM560.1.
Johnson, H. K., J. Hoejstrup, H. J. Vested, and S. E. Larsen (1998), On the dependence of sea surface roughness on wind waves, *J. Phys. Oceanogr.*, *28*, 1702–1716.
Kain, J. S. (2004), The Kain-Fritsch convective parameterization: An update, *J. Appl. Meteorol.*, *54*, 170–181.
Kang, H.-S., and S.-Y. Hong (2008), Sensitivity of the simulated East Asian summer monsoon climatology to four convective parameterization schemes, *J. Geophys. Res.*, *113*, D15119, doi:10.1029/2007JD009692.
Lee, D.-K., H.-S. Kang, and K.-H. Min (2002), The role of ocean roughness in regional climate modeling: 1994 East Asian summer monsoon case, *J. Meteorol. Soc. Jpn*, *80*, 171–189.
Lee, D.-K., Y.-I. Ahn, and C.-J. Kim (2004), Impact of ocean roughness and bogus typhoons on summertime circulation in a wave-atmosphere coupled regional climate model, *J. Geophys. Res.*, *109*, D06112, doi:10.1029/2003JD003781.
Lee, M.-I., S. Schubert, M. Suarez, I. Held, Ng. Lau, J. Ploshay, A. Kumar, H. K. Kim, and J. Schemm (2007), An analysis of the warm-season diurnal cycle over the continental United States and Northern Mexico in general circulation models, *J. Hydrometeorol.*, *8*, 344–366.
Mlawer, E. J., S. J. Taubman, P. D. Brown, M. J. Iacono, and S. A. Clough (1997), Radiative transfer for inhomogeneous atmospheres: RRTM, a validated correlated-k model for the long wave, *J. Geophys. Res.*, *102*, 16,663–16,682, doi:10.1029/97JD00237.
Moon, I.-L., I. Ginis, T. Hara, and B. Thomas (2007), A physics-based parameterization of air-sea momentum flux at high wind speeds and its impact on hurricane intensity predictions, *Mon. Weather Rev.*, *135*, 2869–2878.
Noh, Y., C. J. Jang, T. Yamagata, P. C. Chu, and C.-H. Kim (2002), Simulation of more realistic upper-ocean processes from an OGCM with a new ocean mixed layer model, *J. Phys. Oceanogr.*, *32*, 1284–1307.
Pollard, R. T., P. B. Rhines, and R. O. R. Y. Thompson (1972), The deepening of the wind-mixed layer, *Geophys. Astrophys. Fluid Dyn.*, *4*, 381–404, 10.1080/03091927208236105.
Powers, J. G., and M. T. Stoelinga (2000), A coupled air-sea mesoscale model: Experiments in atmospheric sensitivity to marine roughness, *Mon. Weather Rev.*, *128*, 208–228.
Reynolds, R. W., N. A. Rayner, T. M. Smith, D. C. Stokes, and W. Wang (2002), An improved in situ and satellite SST analysis for climate, *J. Clim.*, *15*, 1609–1625.
Seo, H., A. J. Miller, and J. O. Roads (2007), The Scripps Coupled Ocean-Atmosphere Regional (SCOAR) model, with applications in the eastern Pacific sector, *J. Clim.*, *20*, 381–402.
Shinoda, T. (2005), Impact of the diurnal cycle of solar radiation on intraseasonal variability in the western equatorial Pacific, *J. Clim.*, *18*, 2628–2636.
Skamarock, W. C., J. B. Klemp, J. Dudhia, D. O. Gill, D. M. Barker, M. G. Duda, X.-Y. Huang, W. Wang, and J. G. Powers (2008), A description of the advanced research WRF version 3, *Tech. note NCAR/TN−475+STR*, National Center for Atmospheric Research, Boulder, Colorado.
Sutton, R., and P. P. Mathieu (2002), Response of the atmosphere-ocean mixed layer system to anomalous ocean heat flux convergence, *Q. J. R. Meteorol. Soc.*, *128*, 1259–1275.
Stephens, M. Y., R. J. Oglesby, and M. Maxey (2005), A one-dimensional mixed layer ocean model for use in three-dimensional climate simulations: Control simulation compared to observations, *J. Clim.*, *18*, 2199–2221.
Wang, B., Q. H. Ding, X. H. Fu, I.-S. Kang, K. Jin, J. Shukla, and F. Doblas-Reyes (2005), Fundamental challenge in simulation and prediction of summer monsoon rainfall, *Geophys. Res. Lett.*, *32*, L15711, doi:10.1029/2005GL022734.
Wilson, C. A., and J. F. B. Mitchell (1986), Diurnal variation and cloud in a general circulation model, *Q. J. R. Meteorol. Soc.*, *112*, 347–369.
Xie, S.-P, T. Miyama, Y. Wang, H. Xu, S. P. de Szoeke, R. J. O. Small, K. J. Richards, T. Mochizuki, and T. Awaji (2007), A regional ocean-atmosphere model for eastern Pacific climate: Toward reducing tropical biases, *J. Clim.*, *20*, 1504–1522.
Yhang, Y.-B., and S.-Y. Hong (2008), Improved physical processes in a regional climate model and their impact on the simulated summer monsoon circulations over East Asia, *J. Clim.*, *21*, 963–979.
Zeng, X., and A. Beljaars (2005), A prognostic scheme of sea surface skin temperature for modeling and data assimilation, *Geophys. Res. Lett.*, *32*, L14605, doi:10.1029/2005GL023030.

S.-Y. Hong, Department of Atmospheric Sciences, College of Sciences, Yonsei University, 262 Seongsanno, Seodaemun-gu, Seoul, KR-120-749, Korea. (shong@yonsei.ac.kr)
E.-J. Kim, Numerical Data Assimilation Division, Numerical Prediction Office, Korea Meteorological Administration, Gisang Cheong-Gil, Dongjak-gu, Seoul, KR-156-720, Korea.